Azimuthal correlation between jets and ridges

Charles B. Chiu[*][†]

University of Texas at Austin

E-mail: chiu@physics.utexas.edu

Rudolph C. Hwa

University of Oregon

E-mail: hwa@uoregon.edu

We demonstrate that the trigger-ridge azimuthal correlation in data can be understood based on a phenomenological model, called the Correlated Emission Model. In this model successive soft emissions due to jet-medium interaction lead to the enhancement of thermal partons which follow the local flow directions. The enhanced thermal partons are the source of the ridge particles. The correlation between the flow direction and the trigger direction plays a central role in understanding this azimuthal correlation. Features in the ridge yield at various trigger angles as a function of the relative azimuthal angle between the ridge and the trigger and as a function of the impact parameters are discussed.

Workshop on Critical Examination of RHIC Paradigms

April 14-17, 2010

Austin, Texas, U.S.A.

---

[*]Speaker.

[†]Thanks to the organizing committee for the pleasant atmosphere of the conference and giving me the opportunity to present this talk.

Outline

- 1. Ridge phenomena

- 2. Correlated emission model

    - 2.1 A scenario of ridge formation

    - 2.2 The correlated emission ansatz

    - 2.3 Ridge yield per trigger

- 3. Comparison with the data

    - 3.1 Model fit to the ϕ_s data.

    - 3.2 Comparison with $\Delta\phi$ data at various trigger angles

- 4. Model predictions

    - 4.1 The $\Delta\phi$ curves

    - 4.2 The asymmetry parameter

    - 4.3 R-yield vs b (or Npart) at various trigger angles

- 5. Summary

1. Introduction

This talk is on the azimuthal correlation between jets and ridges based on our published work in ref.[1]. A typical ridge phenomenon we are interested in is illustrated in the 3d plot of Fig.1, where the number of dihadron correlation events is plotted as a function of the azimuthal angular difference $\Delta\phi = \phi_{assoc} - \phi_{trigger}$ and the longitudinal pseudorapidity difference $\Delta\eta = \eta_{assoc} - \eta_{trigger}$.[2].

There the ridge is closely associated to a jet. It has a relatively long stretch in the longitudinal direction. There is a widening of the azimuthal distribution, up to about $\Delta\phi \sim 1$ rad in the azimuthal direction. For the case illustrated the transverse momentum range is semi-hard. More specifically the trigger range is, $3 < p_{Ttrigger} < 4$ GeV, and the associated particles, $p_T > 2$ GeV. There are also other examples of jet triggered ridges with semihard associated particle momenta. See refs.[3, 4, 5].

Ridges also appear in the auto correlation data such as the case shown in Fig.2. Here no distinction between the triggers and associated particles were made. The data illustrated have the transverse momentum range $0.15 < p_T < 2$ GeV. Notice that here $|\Delta\eta|$ extends to about 1.3. The data are for Au+Au collisions at 130 GeV, from ref.[6]. Recently the trigger-ridge azimuthal correlation data became available. This is shown in Fig.3, from ref.[7]. As indicated by the title of this talk, the azimuthal correlation is the main focus of today's presentation. The data shown
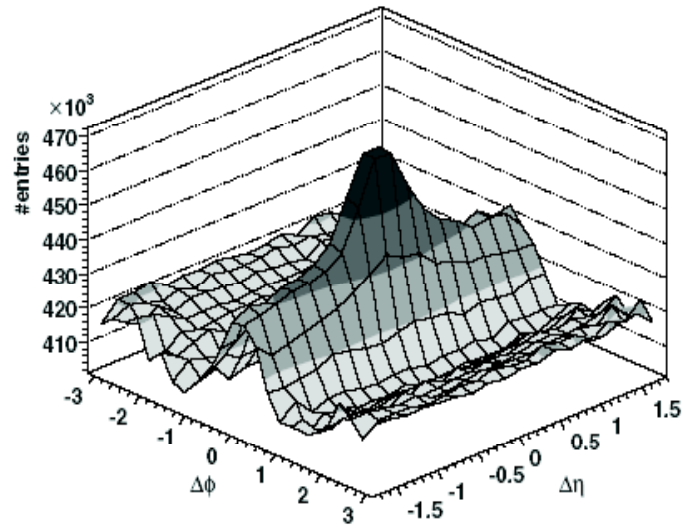
Figure 1: A typical Ridge structure plotted as a function of the longitudinal and the transverse two particle correlation variables: $\Delta\eta$ and $\Delta\phi$. Central region: $3 < p_{Ttrigger} < 4$ GeV, $p_{assoc} > 2$ GeV. From [2].
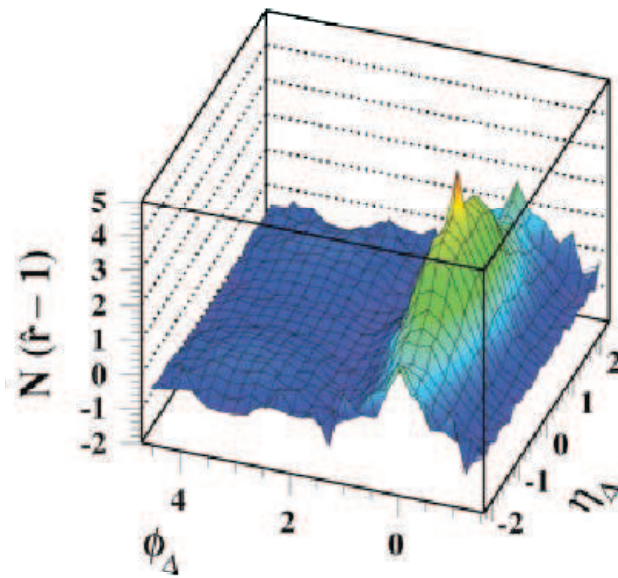
Figure 2: Ridge structure given in auto-correlation data. No distinction is made between triggers and associated particles. From [6].

3

here plays an important role in our investigation. The left figure is for the central region, with the centrality 0-5%. For brevity, hereon this region will be referred to as the C-region and the right figure is for centrality 20-60%, which hereon will be referred to as the noncentral region, or the NC-region. Notice the differences between the two. Compared to the NC case, the C case has
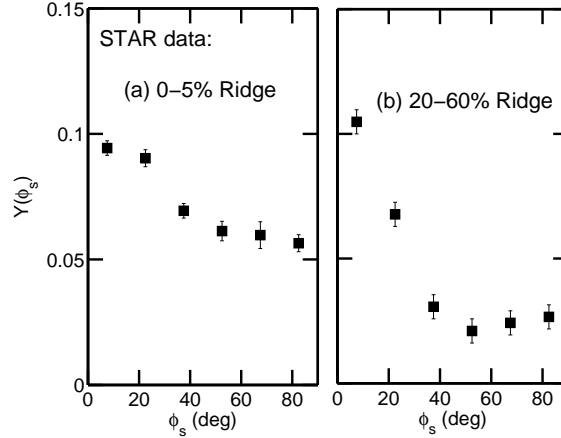
Figure 3: Ridge structure given in auto-correlation data. No distinction is made between triggers and associated particles. From [6].

a milder drop as the trigger angle ϕ_s increases. They both level off at near $90°$ region. We will proceed now to our model.

2. Our model

Let me begin with a qualitative picture, to see how the azimuthal dependence of interest is to be described within our approach.

2.1 A scenario of ridge formation

The processes of interest are from nearside correlation measurements, where the trigger is at mid-rapidity with $3 < p_T^{trig} < 4$GeV/c and the associated particles with $1.5 < p_T^{assoc} < 2$ GeV/c. A typical dihadron correlation process begins with a large p_T jet from a high energy parton-parton collision where the collision takes place near the surface, say at point P (x_0, y_0). Here the hard (or semihard) parton in the jet exits to form the trigger and the recoiled hard parton moves in opposite direction and is absorbed by the medium.

There are successive soft emissions due to jet-medium interaction. It is the absorption of radiative energy by the medium which leads to energizing the local medium-partons, in turn the generation of the enhanced thermal partons. We identify the enhanced thermal partons as the source for the ridge particles. They are carried by the local transverse flow of the medium. The transverse

4

flow direction defines the average direction of the eventual ridge particles. A word of caution is in order here. we do not require thermal equilibrium at early time. The usage of the terms thermal and the enhanced thermal refers to the exponential behaviors of the transverse momentum distributions of the partons at late time just before hadronization.

2.2 The correlated emission ansatz

We assume the strength in the emission of ridge particles is correlated to the relative angle between the flow direction and the trigger direction. Let me begin with the geometry of triggers and flows. Fig. 4 illustrates the situation. The trigger directions are indicated by the thin arrows. a) is for the trigger angle of $\phi_s = 0°$. 3 different starting points are indicated. Each has a local flow direction (indicated by the thick green arrow associated with it, along the direction ψ_s). Only the middle one corresponds to the matched case, where the flow direction is aligned with the trigger direction, i.e. $\psi = \phi$. b) is for $\phi_s = 70°$. Here the matched case occurs at the upper one.
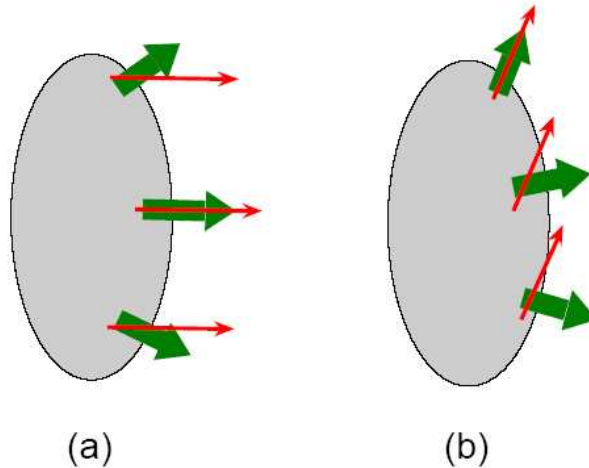
Figure 4: (Color online) Illustrations of the relationship between the trigger directions ϕ_s in (red) arrows and the flow directions ψ in thick (green) arrows for noncentral collision. (a) Semihard partons at $\phi_s = 0$ originated from 3 different points P where only the middle one has matching ϕ_s and ψ that lead to strong ridge, while in (b) for $\phi_s \sim 70°$ only the upper one has matching angles, leading to stronger ridge than in the two lower non-matching cases, but it is weaker than the middle one in (a) because of lower local density at the tip of the ellipse.

For the matched case, here enhanced thermal partons which are the potential ridge particles are aligned in the same direction. We assume the reinforcement of the flow enhances the emission of ridge particles. The totally mismatched situation will be the case where the flow direction is perpendicular to the trigger direction. Here potential ridge particles formed at different hard-parton-

mediun interaction points are emitted along different directions. Due to the lack of coherence, the ridge yield is expected to be suppressed.

The correlated emission ansatz states that the ridge yield favors the matched case and suppresses the mismatched case. Quantitatively this effect is represented by a gaussian function in the angular difference variable, i.e.

$$C(x,y,\phi_s) = \exp\left[-\frac{(\phi_s - \psi(x,y))^2}{2\lambda}\right] , \qquad (2.1)$$

where λ is a parameter to be determined. This is a phenomenological formula that cannot be derived from first principles, but has a sound physical basis and will play a central role in our model. For every point (x,y) on the trajectory, the flow direction $\psi(x,y)$ specifies only the average direction of the ridge hadrons. Since there are statistical fluctuations, the magnitude of which depends on how far (x,y) is away from the surface along the direction $\psi(x,y)$. That distance is t'. We introduce another Gaussian form to describe the mentioned fluctuation of the azimuthal angle ϕ of a ridge particle from the average flow direction

$$\Gamma(x,y,\phi) = \exp\left[-\frac{(\phi - \psi(x,y))^2}{2\gamma t'}\right] , \qquad (2.2)$$

where the degree of fluctuation is specified by $\gamma t'$, which is the square of the gaussian width. Clearly, the farther the emission point from the surface, the wider ϕ fluctuates from $\psi(x,y)$.

2.3 Ridge yield per trigger

The probability of ridge yield at ϕ initiated from a trigger starting from the interaction point (x_0,y_0) and emerging at angle ϕ_s, is given by

$$R(\phi,\phi_s,x_0,y_0) = NP(x_0,y_0,t)t \times \int_0^1 d\xi D(x_\xi,y_\xi)C(x_\xi,y_\xi,\phi_s)\Gamma(x_\xi,y_\xi,\phi) , \qquad (2.3)$$

where N is an overall normalization constant which will be canceled when we compute the yield per trigger. The variables t, x_ξ and y_ξ all depend implicitly on the initial coordinates (x_0,y_0).

Here $P(x_0,y_0,t)$ is the probability of detecting a parton emerging from the medium. It is the product of the probability of producing a semihard parton at (x_0,y_0), which is proportional to the product of the longitudinal lengths at that point, $L_A(x_0,y_0)L_B(x_0,y_0)$, and the survival probability $S(t)$, i.e.,

$$P(x_0,y_0,t) \propto L_A(x_0,y_0)L_B(x_0,y_0)S(t) . \qquad (2.4)$$

The former depends on the nuclear matter density assumed, which we will not detail here. Due to the opaqueness of the dense medium, a sharp suppression factor as t increases is expected. We represent the survival probability as

$$S(t) = exp(-t/t_0) \qquad (2.5)$$

The final expression of ridge yield per trigger after integrating over all interaction points in the overlap almond is given by

$$R(\phi, \phi_s) = \frac{\int dx_0 dy_0 R(\phi, \phi_s, x_0, y_0)}{\int dx_0 dy_0 P(x_0, y_0, t)} \ . \tag{2.6}$$

3. Comparison with the data

3.1 Model fit to the ϕ_s data.

The expressions given in subsections 2.2 and 2.3 define our model. The main parameter of the model is t_0 which characterizes the thickness of the interaction layer and λ the square of the gaussian width which characterizes the correlation between the trigger direction and the flow direction.

Fig.5 shows our fit to the data, where $t_0 = 0.2$ or the interaction layer is about $R_A/5$ and $\lambda = 0.11$ or the correlation angle about 20 deg. Notice that for the C case, the model reproduces
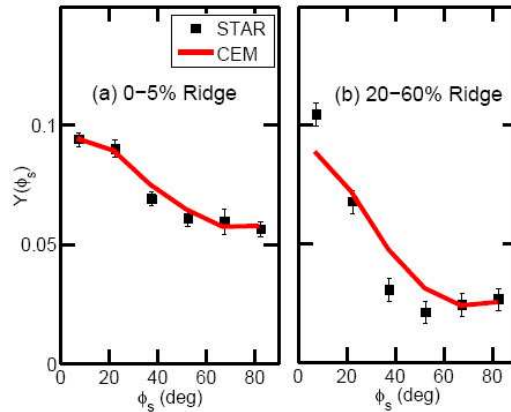
Figure 5: (Color online) Dependence of ridge yield on ϕ_s for (a) top 5% and (b) 20-60%. Data are from Ref. [7]. The solid lines are the results of calculation in CEM.

the mild azimuthal dependence. It fits to the azimuthal distribution well including the flattening feature near 90 deg. For the NC-region, the predicted curve has a steeper slope and a flattening feature near 90 deg, qualitatively describes the feature of the data.

One can qualitatively understand the contrast in the slopes between the C-case and the NC case from the geometry shown in Fig.6. The left column is for the C-region and the right column for the NC-region. Consider the situation of the top row. Here $\phi_s \sim 0°$. For both C and NC cases, the flow direction is more or less aligned with the trigger direction. Comparable yields for C and for NC are expected. The bottom row is at a larger trigger angle, say in the neighborhood of $\phi_s = 70deg$. Due to elliptic geometry for the NC-case, the NC case has a more pronounced mismatch compared to the C-case. Also in this region the NC case has a less matter medium compared to the C case.

7
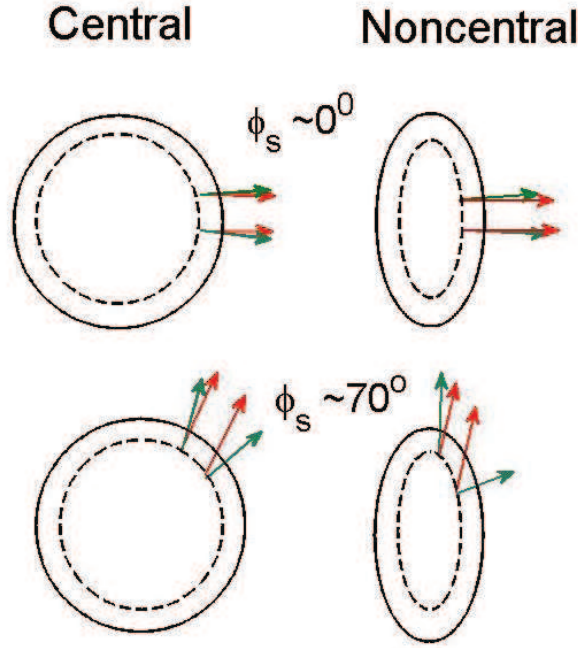
Figure 6: A comparison of the misalignment situation between the C case and the NC case. Near $\phi_s \sim 0$ region, both dominated by the alignment configuration. At around $\phi_s \sim 70°$, for the NC case, the elliptic geometry makes the misalignment effect more noticeable, it causes a stronger suppression in the ridge yield.

Thus the NC case leads a larger drop in the azimuthal dependence. Notice that at the trigger angle $\phi_s = 90°$, it is the matched case, where the flow aligns with the trigger. The ϕ_s dependence is symmetric about 90 deg, which is responsible for the flatness of the azimuthal dependence near 90 deg.

3.2 Comparison with $\Delta\phi$ data at various trigger angles

Fig.7b shows the ridge yield as a function of difference $\Delta\phi = \phi_{ridge} - \phi_{trigger}$ at the trigger angle $\phi_s = |22°|$. The predicted curve agrees with the data. Instead of combining the ridge contribution for the absolute value of the trigger angles, ± 22 deg, Fig.7a shows the predicted curve for $\phi_s = 22°$ case and a separate curve for $\phi_s = -22°$. Notice that there is noticeable shift in the peak positions between the two cases. There is a geometric reason for this shift, which will be discussed in the following section.
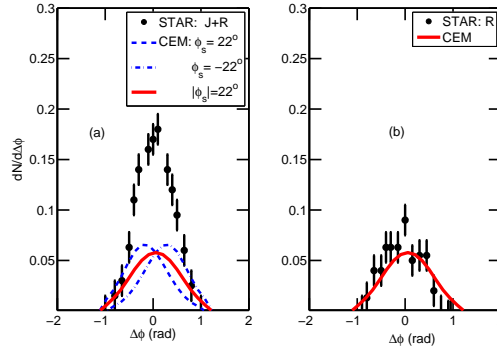
Figure 7: (Color online) The data are $\Delta\phi$ distributions from [7] for $15 < \phi_s < 30°$ at 20-60% centrality for (a) the sum of jet and ridge and (b) ridge alone. The curves are all calculated in the CEM for the ridge distributions only with $\gamma = 1$. The dashed and dashed-dotted lines are left- and right-shifted for $\phi_s = \pm 22°$, respectively. The solid lines are the average over the two signs of ϕ_s.

4. Model predictions

4.1 The $\Delta\phi$ curves

The $\Delta\phi$ curves of ridge yield at various trigger angles $\phi_s = 7, 22, 37, 52, 67$ and 82 deg are shown in Fig.8. Notice how the height and the peak position vary as the trigger angle increases.
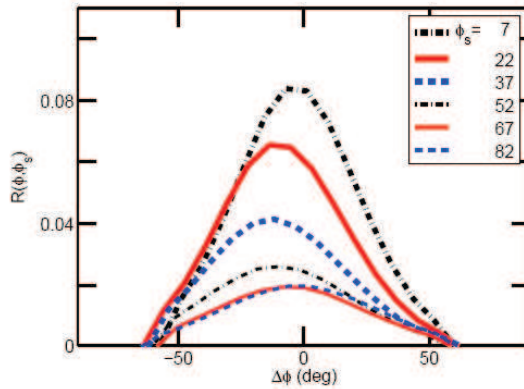
Figure 8: (Color online) The ridge distributions for various positive values of ϕ_s.

More specifically, there is a systematic shift to the left in the peak position as the trigger angle increases, with the maximum shift occurring at around $\phi_s = 37$ deg, where the magnitude of the shift is approximately $|\Delta\phi| = 10$ deg. As the trigger angle further increases, there is a gradual shifted to the right. The shift of the peak decreases to 0 deg, as the trigger angle approaches 90 deg.

4.2 The asymmetry parameter

To characterize the variation in the skewness of the curves, we work with the asymmetry parameter defined by

$$A(\phi_s) = \frac{Y_+(\phi_s) - Y_-(\phi_s)}{Y_+(\phi_s) + Y_-(\phi_s)} \,, \tag{4.1}$$

For the trigger angle in the range 0 to $\pi/2$,

$$Y_+(\phi_s) = \int_{\phi_s-1}^{\phi_s} d\phi R(\phi, \phi_s), \tag{4.2}$$

$$Y_-(\phi_s) = \int_{\phi_s}^{\phi_s+1} d\phi R(\phi, \phi_s) \,. \tag{4.3}$$

Notice that Y_+ represents the ridge yield for $\Delta\phi \leq 0$. Inspection of the curves shown in Fig.8 indicates that at within the trigger angle range shown, $A \geq 0$. When the trigger angle is 0, there is the symmetry $\Delta\phi = -\Delta\phi$, which implies that $Y_+ = Y_-$, or A=0. By the same token, at $\phi_s = 90$ deg there is again the symmetry $\Delta\phi = -\Delta\phi$ which again leads to A=0. Fig.9 shows the predicted curves of A versus ϕ_s, where the dashed curve is for the C-region case and the solid curve for the NC-region case. Our work led to the subsequent analysis of the STAR data, the result of which was
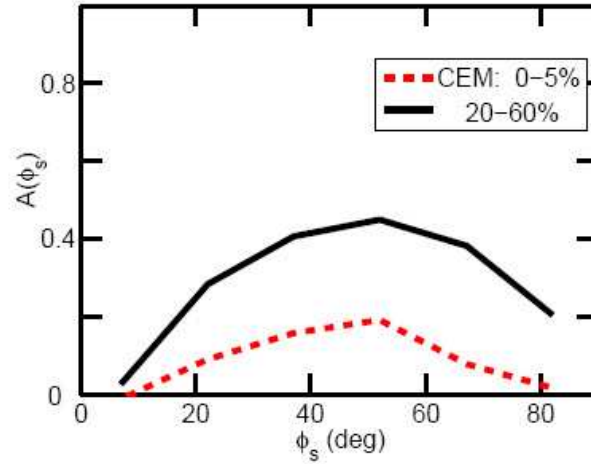
Figure 9: (Color online) The asymmetry function $A(\phi_s)$ for 0-5% (dashed) and 20-60% (solid).

reported at QM09[8]. Fig.10 shows a comparison between their data and the CEM predicted curve for the NC-case. One sees that the data confirms the qualitative feature predicted by our model.

4.3 R-yield vs b (or Npart) at various trigger angles

Fig.11 shows the ridge yield as a function of the normalized impact parameter b/R, where R is the effective radius of the colliding nucleus (Au). R=7fm is used. Fig.11a gives an overview
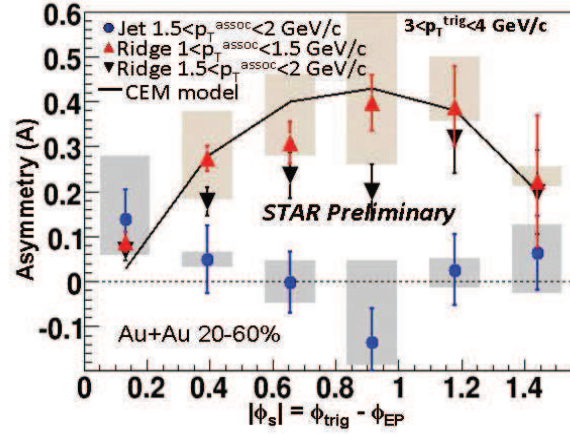
Figure 10: A vs ϕ_s: The recent STAR data, the triangular and inverted triangular points, [8] compared to CEM-prediction (solid curve).

of the b-dependence of the ridge yield curves at trigger angles: 5, 20, 40, 60 and 80. Fig.11b is the averaged ridge yield vs b, where the average is over the trigger angles. Fig.11c is the averaged ridge yield vs N_{part}. Two averaged ridge yield points taken from the STAR data are included for comparison.

Notice as shown in Fig.11b,c, after averaging over the trigger angles, the yield decreases monotonically with b (or it increases monotonically with N_{part}). We stress that the smooth monotonic variation in b or N_{part} occurs only after averaging over the trigger angles is made. In the small trigger angle region, for the b-curves the variation in b is not monotonic. There is a bump in the intermediate b region.

The bump here has a geometric origin. Fig.12 illustrates the situation for trigger angle, $\phi_s = 0$ deg. First consider the b=0 case. Here the right-half of the overlap of the almond in the initial state is represented by a semicircle. The interaction region is shown as the thick band of a semicircular arc. The interaction domain may schematically be divided into two regions I, and II. Region I represents the bulk region of interaction. In this region, the flow directions are to mostly aligned with the trigger direction. There is a large ridge yield. Region II is the polar cap region. Here the flow direction is predominantly misaligned with respect to the trigger direction. The ridge yield is highly suppressed. So for the present b=0 case, the yield per trigger is schematically given by: Ridge-yield(b=0)~I/(I+II). We now turn to the intermediate b region case (or the larger b case as indicated in the figure). The situation for this case is also illustrated in Fig.12. Here the initial overlap region is represented by the right half of a narrow almond. Here the vertical chord, which defines the left border of the narrow almond has been moved to the right by a significant amount compared to the b=0 case. Here much of the polar cap region has been eliminated. The yield per

11
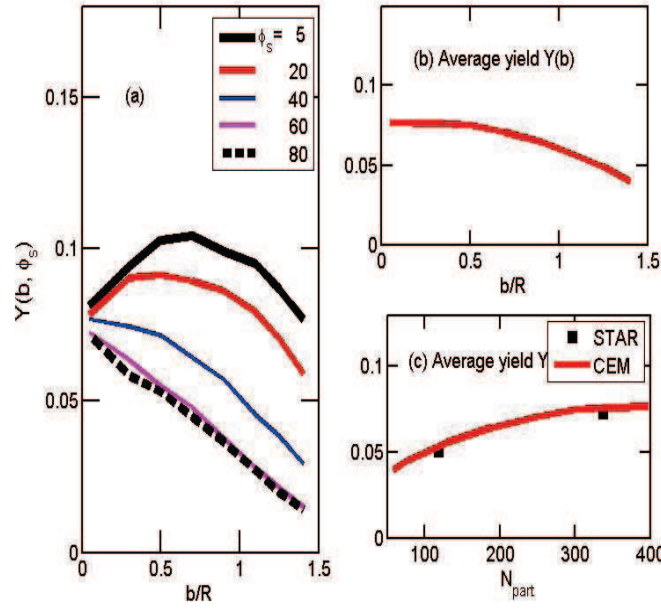
Figure 11: (Color online) (a) Ridge yield per trigger vs impact parameter for 5 values of ϕ_s, (b) $Y(b)$, averaged over all ϕ_s, vs impact parameter, and (c) average yield vs N_{part}. The two points in (c) are determined from the data in Fig. 2(a) and (b).
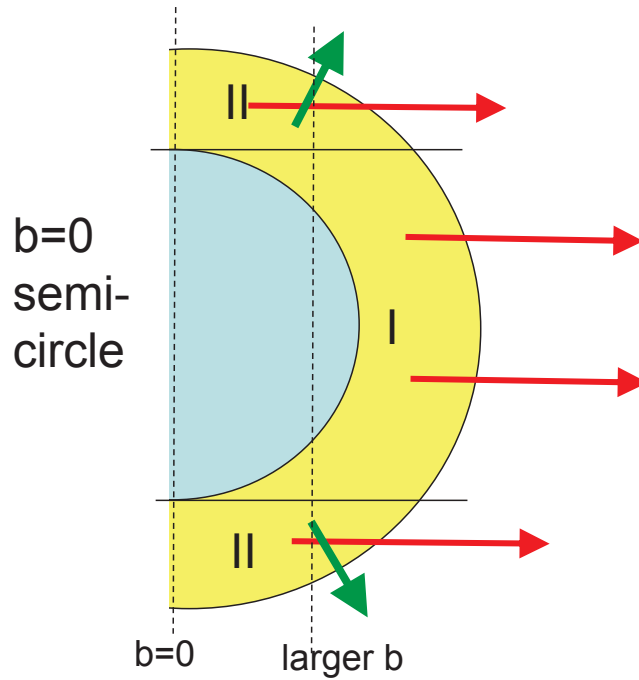
Figure 12: The geometry illustrating the origin for the increase of the ridge yield from b=0 to intermediate b value, when the trigger angle is 0.

trigger may be schematically represented by: ridge-yield (larger b case)=$I/(I + \varepsilon II)$ where ε is a small number compared to unity. Thus the yield per trigger in the larger b region is greater than that at b=0, which causes a hump in this b region. This is the situation for 0 deg trigger angle. As the trigger angle increases, the bump becomes less and less pronounced. At around $\phi_s = 30°$ the hump structure disappears completely, this marks the onset of a smooth monotonic decrease of the yield-curve. It is interesting to see whether future data will confirm the prediction here.

5. Summary

We see the ridge data have provided strong evidence that the medium response in jet-medium interactions depends on the direction of the transverse flow of the medium. The flow influences the direction in which the loss of energy should go and where the ridge should be formed. CEM uses the presence of the ridge as a means to keep track of the energy loss of the jets going into the medium. We have found that the ridge formation can be strong only within 20 deg around the trigger direction. When the flow is perpendicular to the jet direction, the ridge yield is completely suppressed.

We have shown that the CEM reproduces the ϕ_s dependence of the ridge yield data. Our study allows us to predict the trigger angle dependence of the asymmetry parameter which has subsequently been confirmed by the data. Our study also predicts the impact parameter dependence (or b-dependence) of the ridge yield. Our b-curve averaging over the trigger angles agrees with the data. We have also presented b-curves at various trigger angles for verification in the future.

In this talk our focus has been on the ridge-trigger correlations in the transverse direction. Our investigation on the longitudinal correlation is in progress. After my presentation, there were several followup questions and comments related to the longitudinal correlation. I refer the reader to my contribution of [Note added] to the Saturday QA session, in which the longitudinal correlation problem related to our CEM model is briefly discussed.

References

[1] C. B. Chiu and R. C. Hwa, Phys.Rev. C **79**, 034901(2009); arXiv:0809.3018.

[2] J. Putschke (for STAR Collaboration), J. Phys. G **34**, S679 (2007).

[3] C. Suarez, (for STAR Collaboration), poster at Quark Matter 2008, Jaipur, India (2008).

[4] J. Bielcikova (for STAR Collaboration), talk given at Winter Meeting on Nuclear Physics, Bormio, Italy (2008).

[5] C. Nattrass for the START collaboration, arXiv 0809.5261.

[6] M. Daugherity (STAR), a talk given at Quark Matter 2008; see also J. Adams, STAR, PRC, 064907 (2006).

[7] A. Feng, (for STAR Collaboration), talk given at Quark Matter 2008, Jaipur, India (2008), J. Phys. G: Nucl. Part. Phys. **35**, 104082 (2008), arXiv: 0807.4606.

[8] P. K. Netrakanti (STAR), Nucl. Phys. A830:681c, 2009; arXiv: 0907.4744.

PoS(CERP2010)028